specific impulse of 1800 sec. The best over-all efficiency was 20% at a specific impulse of 1800 sec. It is estimated that simple thermal design cleanup of cathode and vaporizer units will allow operation at 140 w/mlb and 29% overall efficiency at 1800 sec. Preliminary testing with several electrostatic thrust vectoring concepts has resulted in the identification of some critical operational problems without a successful demonstration of beam vectoring. No fundamental barriers have been identified, however, and the investigation of electrostatic vectoring is proceeding.

References

[1] Boucher, R. A., "Electrical Propulsion for Control of Stationary Satellites," *Journal of Spacecraft and Rockets*, Vol. 1, No. 2, March-April 1964, pp. 164–169.

[2] Duck, K. I., Bartlett, R. O., and Sullivan, R. J., "Evaluation of an Ion Propulsion System for a Synchronous Spacecraft Mission," AIAA Paper 67-720, New York, 1967.

[3] Rawlin, V. K. and Kerslake, W. R., "SERT II: Durability of the Hollow Cathode and Future Applications of Hollow Cathodes," *Journal of Spacecraft and Rockets*, Vol. 7, No. 1, Jan. 1970, pp. 14–20.

[4] Banks, B. A., "A Fabrication Process for Glass Coated Electron-Bombardment Ion Thruster Grids," TN D-5320, 1969, NASA.

[5] Keller, T. A., "NASA Electric Rocket Test Facilities," *Seventh National Symposium on Vacuum Technology Transactions*, edited by C. R. Meisner, Pergamon Press, New York, 1961, pp. 161–167.

[6] Byers, D. C. and Staggs, J. F., "SERT II: Thruster System Ground Testing Performance," *Journal of Spacecraft and Rockets*, Vol. 7, No. 1, Jan. 1970, pp. 7–14.

[7] Margosian, P. M., "Preliminary Tests of Insulated Accelerator Grids for Electron Bombardment Thrustor," TM X-1342, 1967, NASA.

[8] Nakanishi, S., Richley, E. A., and Banks, B. A., "High-Perveance Accelerator Grids for Low-Voltage Kaufman Thrustors," *Journal of Spacecraft and Rockets*, Vol. 5, No. 3, March 1968, pp. 356–358.

[9] Lathem, W. C. and Staggs, J. F., "Divergent-Flow Contact-Ionization Electrostatic Thrustor for Satellite Attitude Control and Station Keeping," TN D-4420, 1968, NASA.

NOVEMBER 1970 J. SPACECRAFT VOL. 7, NO. 11

Aerodynamic Design of Axisymmetric Hypersonic Wind-Tunnel Nozzles

JAMES C. SIVELLS*
ARO Inc., Arnold Air Force Station, Tenn.

A unified approach to nozzle design is presented in which an inviscid contour is first determined and then corrected to account for the growth of a turbulent boundary layer along the contour. The inviscid contour is obtained by the axisymmetric method of characteristics from a prescribed distribution of velocity along the nozzle axis. The velocity distribution matches theoretical transonic conditions at the throat, conical-source flow conditions through an intermediate region, and design flow conditions at the nozzle exit. The second derivative of the axial velocity is continuous throughout and is zero at the exit point. The interdependence of some of the nozzle parameters is discussed. A semiempirical method is presented for calculating the boundary-layer correction. Calculated values agree within about 15% with experimental values obtained in 50-in.-diam, water-cooled nozzles over a Mach number range of 6 to 10.

Nomenclature

A^* = sonic area
a_e, a_0 = speed of sound at T_e and T_0, respectively
$B_{1,2}$ = coefficients in Eq. (73)
C_{1-4} = coefficients in Eq. (28)
C_f, C_{fi} = skin-friction coefficients, compressible and incompressible flow
D_{0-5} = coefficients in Eq. (37)
F_c $\equiv T'/T_e$
G_n = integrating factor for nth point
H = boundary-layer form factor, δ^*/θ
H_i = form factor, incompressible flow
K = square root of mass flow ratio
k $\equiv (\gamma + 1)/(\gamma - 1)$
M = Mach number
R = ratio of throat radius of curvature to throat radius
R_1 $\equiv r_1/r^*$
R_{x_e} = freestream Reynolds number based on x
R_θ, R_{θ_i} = compressible and incompressible Reynolds numbers based on momentum thickness
r = radial distance from source
r_1 = value of r when $M = 1$
r^* = radius of geometric throat
S $\equiv R + 1$
s $\equiv x_{n-1} - x_{x-2}$
T, T_s = static and stagnation temperatures within boundary layer
T_{aw} = adiabatic wall temperature
T_e, T_0 = freestream static and stagnation temperatures
T_w = wall temperature
T' = reference temperature
t $\equiv x_n - x_{n-1}$
U, U_e = transformed velocities within and at edge of boundary layer
u, u_e = velocities within and at edge of boundary layer
W = (velocity)/(velocity at sonic point)
X_E $\equiv (x_E - x_I)/r_1$
x = axial distance from source [except Eqs. (12, 14, and 17)]
Y = transformed distance normal to surface
y = distance normal to axis
α = factor in Eq. (62)

Presented as Paper 69-337 at the AIAA 4th Aerodynamic Testing Conference, Cincinnati, Ohio, April 28–30, 1969; submitted May 14, 1969; revision received August 17, 1970. The research reported herein was sponsored by the Arnold Engineering Development Center, Arnold Air Force Station, Tenn., under Contract F40600-70-C-0001 with ARO, Inc. Reproduction to satisfy the needs of the U.S. Government is authorized.

* Staff Engineer, Aerodynamics Division, von Kármán Gas Dynamics Facility. Associate Fellow AIAA.

β $\equiv [2/(\gamma + 1)R]^{1/2}$
γ = ratio of specific heats
Δ = edge of boundary layer
δ^* = boundary-layer displacement thickness neglecting transverse curvature effects
$\delta_a{}^*$ = axisymmetric displacement thickness
ϵ = sonic point displacement distance, Fig. 1
ζ $\equiv (x - x_I)/(x_E - x_I)$
θ = boundary-layer momentum thickness
λ $\equiv [2/(\gamma + 1)S]^{1/2}$
μ_e, μ_w = viscosities at T_e and T_w, respectively
ξ $\equiv (x - x_B)/(x_C - x_B)$
ρ_e, ρ_0 = density of T_e and T_0, respectively
ϕ = wall angle at edge of inviscid contour
ψ = Prandtl-Meyer expansion angle, two-dimensional flow
ψ' = expansion angle in radial flow
ω = wall angle at inflection point

Subscript

A,etc. = value of quantity at point designated in Fig. 1

Introduction

THE aerodynamic design of wind-tunnel nozzles has evolved from the two-dimensional type used for supersonic testing to the axisymmetric type as the test Mach number has increased into the hypersonic regime. Even at Mach 4, the designers of low-density tunnels[1] turned to axisymmetric nozzles because of the adverse effects on the boundary layer produced by the transverse pressure gradients inherent on the side walls of two-dimensional nozzles. At higher Mach numbers, the use of axisymmetric nozzles alleviates the throat design problems caused by the combination of high stagnation enthalpies and large area ratios.[2]

Before the advent of high-speed digital computers, it was extremely time-consuming[2] to calculate the nozzle flow by the axisymmetric method of characteristics.[3] To save time, Foelsch[4] assumed radial (source) flow to exist in a region of the nozzle and developed an approximate method of converting the radial flow to uniform flow. Beckwith et al.[2] showed that Foelsch's approximations were quite inaccurate but utilized the idea of a region of radial flow followed immediately on the axis by uniform flow. This procedure produces a discontinuity in velocity (or Mach number) gradient on the axis, which in turn produces a discontinuity in curvature on the contour.[5] These discontinuities were eliminated by Yu[5] and Cresci[6] by following the radial flow region with a region in which the streamline velocity (or Mach number) gradients are continuously reduced from the radial-flow values to zero at the beginning of parallel flow.

In 1958, a 50-in.-diam Mach 8 nozzle was designed and built for the von Kármán Gas Dynamics Facility at the Arnold Engineering Development Center. This nozzle[7] incorporated a downstream contour developed by Cresci,[6] a semicubic throat contour, and a boundary-layer correction obtained by the method of Ref. 8. The success of this nozzle led to the design and construction of a 50-in.-diam Mach 10 wind tunnel that became operational in 1961. As described in Ref. 7, the downstream contour was so designed that an additional throat section could be used to produce a Mach 12. Both throat sections have a semicubic contour. The flow at both Mach numbers is considered to be satisfactory.

Later, a method was developed for computing the supersonic part of a throat contour by the method of characteristics combined with the transonic solutions of Hall.[9] With the development of the method of computing the throat contour and a modification of Cresci's method for the downstream contour, the general approach to the inviscid aerodynamic design of hypersonic nozzles becomes unified. This approach is presented herein, along with some recent modifications to the method of Ref. 8, for calculating the turbulent boundary-layer correction to the inviscid contour. If the boundary layer is laminar, the method of Ref. 10 can be used to correct the inviscid contour. The inviscid throat contours of two of the nozzles described in Ref. 10 were designed by the method to be described.

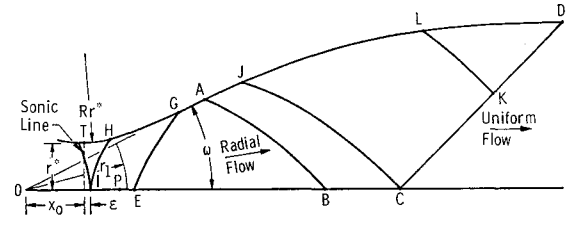

Fig. 1 Regions of inviscid contour.

Inviscid Contour Design

In spite of the advances in transonic flow theory, computational difficulties are experienced[11] in using the method of characteristics starting with an assumed shape of the sonic surface and the shape of the wall in the vicinity of the throat. On the other hand, once an axial velocity distribution has been specified, the method of characteristics can be used to obtain a contour that will produce the prescribed velocity distribution. Improvements in contours thus depend upon improvements in the selection of the axial velocity distribution. The transonic solution is used merely to relate the throat radius ratio R with the displacement ϵ of the sonic point on the axis from the geometric throat and with the derivatives of the axial velocity distribution at the sonic point.

In the present method, the axial velocity distribution is divided into three parts as illustrated in Fig. 1. From sonic point I to point E, where radial flow is assumed to begin, the velocity distribution is described by a fourth-degree polynomial. From point E to point B, radial flow is assumed. From point B to point C, where uniform flow begins, the Mach number distribution is described by a fifth-degree polynomial. The coefficients of the polynomials are chosen such that the second derivative of the axial velocity is continuous throughout and is zero at point C.

In Refs. 2 and 12, a linear distribution in M was used between points I and E, and points G and A were coincidental as were points B and C. The use of a radial-flow region is preferred over designs[1,13,14] that define the axial distribution between points I and C with a single equation, in that the inflection point is well defined with the wall angle at the inflection point as one of the nozzle parameters. The conical region from point G to point A is useful for nozzles designed for high Mach numbers.[15] Also, real-gas effects are more pronounced upstream of point G than downstream where the flow will have expanded to near ideal-gas conditions. Real-gas effects can be taken into account in the characteristics solution as in Ref. 12 and will not be considered hereinafter.

Since radial flow is assumed between points E and B, radial flow exists between the characteristics EG and AB, and the contour from point G to point A is a straight line at an angle ω relative to the axis. Two characteristics solutions are thus needed, one to determine the throat contour from point H on the branch line (characteristic from sonic point I) to point G and the other to determine the downstream contour from point A to the theoretical end of the nozzle, point D. The characteristic CD is a straight line since it defines the beginning of the uniform flow region.

In the following discussion, it is sometimes convenient to use M and, at other times, the velocity ratio W, which are related by

$$W^2 = kM^2/(k - 1 + M^2) \quad (1)$$

In the radial-flow region, the distance r, measured from the source, is related to the local Mach number by

$$(r/r_1)^2 = M^{-1}[(k - 1 + M^2)/k]^{k/2} \quad (2)$$

or to the local velocity ratio by

$$(r/r_1)^2 = W^{-1}[(k-1)/(k-W^2)]^{(k-1)/2} \quad (3)$$

where r_1 is the value of r when $M = W = 1$. By differentiating

$$M' = dM/d(r/r_1) = 2M(k-1+M^2)r_1/(k-1)(M^2-1)r \quad (4)$$

or

$$W' = 2W(k-W^2)r_1/k(W^2-1)r \quad (5)$$

By differentiating again

$$M'' = \frac{-(M')^2[3k-3+6M^2+(k-3)M^4]}{2M(k-1+M^2)(M^2-1)} \quad (6)$$

$$W'' = \frac{-(W')^2[3k-6W^2+(k+2)W^4]}{2W(k-W^2)(W^2-1)} \quad (7)$$

By differentiating one more time

$$\frac{W'''}{(W')^3} = \frac{-W''[2k+3(k-1)W^2+(k-3)W^4]}{(W')^2W(k-W^2)(W^2-1)} + \frac{2[3-(k+2)W^2]}{(k-W^2)(W^2-1)} \quad (8)$$

This third derivative will be discussed later as a criterion. On the axis, $x = r$, since x is also measured from the source.

Furthermore, in the radial flow region,[4] the expansion angle ψ' in radial flow is one-half the Prandtl-Meyer expansion angle ψ in two-dimensional flow

$$2\psi' = \psi = k^{1/2}\tan^{-1}[(M^2-1)/k]^{1/2} - \tan^{-1}(M^2-1)^{1/2} \quad (9)$$

Therefore, the Mach numbers at points E and G, and at points A and B are related by

$$\psi_G = \psi_E + 2\omega,\ \psi_B = \psi_A + 2\omega \quad (10)$$

Obviously, if points A and G coincide

$$\psi_B = \psi_E + 4\omega \quad (11)$$

which is the case for many contours and represents a limiting condition on the selection of parameters. From flow separation considerations, ω is usually no more than 15°, and a common value for many nozzles is 12°.

In the throat region, the axial velocity distribution is related to the radius of curvature Rr^* at the throat according to Hall's transonic solution,[9] which is in the form of a series in $1/R$ and x/r^* where x, in this case, is measured from the geometric throat

$$W = 1 - \frac{1}{4R} + \frac{10\gamma+57}{288R^2} - \frac{2708\gamma^2+7839\gamma+14211}{82944R^3} + \ldots + \frac{x\beta}{r^*}\left(1 - \frac{5}{8R} + \frac{92\gamma^2+180\gamma+639}{1152R^2} + \ldots\right) + \left(\frac{x\beta}{r^*}\right)^2\left(-\frac{2\gamma-3}{6} + \frac{13\gamma-27}{48R} + \ldots\right) + (x\beta/r^*)^3(4\gamma^2-57\gamma+27)/144 + \ldots \quad (12)$$

Hall states that, with the number of terms retained in Eq. (12) and neglecting higher order terms, his solution is the same for nozzles with circular-, parabolic-, and hyperbolic-shaped throats. However, the lack of higher order terms probably limits its usefulness to regions fairly close to the throat.

It should be noted that Eq. (12) has been corrected according to Kliegel and Levine,[16] who found some errors in Hall's work. They also found that Hall's results could be extended to lower values of R by using toroidal coordinates. By substituting the series

$$R^{-1} = S^{-1} + S^{-2} + S^{-3} + \ldots \quad (13)$$

into Eq. (12), the comparable series in $1/S$ and x/r^* is obtained

$$W = 1 - \frac{1}{4S} + \frac{10\gamma-15}{288S^2} - \frac{2708\gamma^2+2079\gamma+2115}{82944S^3} + \ldots + \frac{x\lambda}{r^*}\left(1 - \frac{1}{8S} + \frac{92\gamma^2+180\gamma-9}{1152S^2} + \ldots\right) + \left(\frac{x\lambda}{r^*}\right)^2\left(-\frac{2\gamma-3}{6} - \frac{\gamma+1}{16S} + \ldots\right) + (x\lambda/r^*)^3(4\gamma^2-57\gamma+27)/144 + \ldots \quad (14)$$

For finite values of the radius ratio R, the sonic line is curved as illustrated in Fig. 1. The sonic point on the axis is located downstream of the geometric throat by the amount

$$\frac{\epsilon}{r^*} = \frac{1}{4\beta R}\left(1 - \frac{4\gamma+21}{72R} + \frac{412\gamma^2+1134\gamma+1557}{10368R^2} + \ldots\right) \quad (15)$$

or, in terms of S

$$\frac{\epsilon}{r^*} = \frac{1}{4\lambda S}\left(1 - \frac{4\gamma-15}{72S} + \frac{412\gamma^2+270\gamma+909}{10368S^2} + \ldots\right) \quad (16)$$

Equation (15) may be compared to Sauer's approximation,[17] $\epsilon/r^* = \frac{1}{4}\beta R$.

If x is measured from the sonic point I and nondimensionalized by r_1 instead of r^*, Eqs. (12) and (14) may be rewritten as

$$W = 1 + (x/r_1)W_I' + (x/r_1)^2W_I''/2 + (x/r_1)^3W_I'''/6 + \ldots \quad (17)$$

where

$$W_I' = \beta R_1\left(1 - \frac{4\gamma+9}{24R} + \frac{652\gamma^2+1743\gamma+1629}{6912R^2} + \ldots\right) \quad (18)$$

$$W_I'' = (\beta R_1)^2[1 - 2\gamma/3 + (4\gamma^2-5\gamma-81)/96R + \ldots] \quad (19)$$

and

$$W_I''' = (\beta R_1)^3[(4\gamma^2-57\gamma+27)/24 + \ldots] \quad (20)$$

or, in terms of S

$$W_I' = \lambda R_1\left(1 - \frac{4\gamma-3}{24S} + \frac{652\gamma^2+15\gamma+333}{6912S^2} + \ldots\right) \quad (21)$$

$$W_I'' = (\lambda R_1)^2[1 - 2\gamma/3 + (4\gamma^2-69\gamma+15)/96S + \ldots] \quad (22)$$

and

$$W_I''' = (\lambda R_1)^3[(4\gamma^2-57\gamma+27)/24 + \ldots] \quad (23)$$

It may be recognized that β is the velocity gradient W_I'/R_1 obtained by Sauer (or from a simple one-dimensional analysis). The work of Sauer was extended by Sims[18] for a linear velocity distribution on the axis. Values of ϵ/r^* and W_I'/R_1 are compared in Table 1, for the lowest value of R for which Sims could obtain a solution for $\gamma = 1.4$. As the value of R is increased, the agreement between the various methods becomes better as expected.

Both Sauer and Sims assumed that W_I'' and W_I''' were zero. It may be noted that for $\gamma = 1.4$, $W_I'' = 0$ from Eq.

Table 1 Comparison of values of ϵ/r^* and W_1'/R_1 where $\gamma = 1.4$ and $R = 4.0$

Source	ϵ/r^*	W_1'/R_1
Sauer[17]	0.136931	0.456435
Sims[18]	0.135530	0.428522
Eqs. (15) and (18)	0.127546	0.409088
Eqs. (16) and (21)	0.126662	0.403258

(19) if $R = 12.525$ and from Eq. (22) if $R = 10.525$ and has a maximum positive value of about $0.0012R_1^2$ for $S = 23.05$, whereas $W_1''' \approx -1.425R_1^3/S^{1.5}$. Although the accuracy of these equations is limited by the number of terms retained in Hall's series, the value of W_1''' should not be neglected, and even the value of W_1'' is retained in subsequent equations.

Hall also gives expressions for the radial distribution of both the axial and the radial velocity components in the throat region. These can be used to obtain the ratio K^2 of the actual mass flow through the throat to the one-dimensional value that would be obtained if the sonic line were straight:

$$K^2 = 1 - \frac{\gamma + 1}{96R^2}\left(1 - \frac{8\gamma + 21}{24R} + \frac{754\gamma^2 + 2132\gamma + 2535}{2880R^2} + \ldots\right) \quad (24)$$

This equation has also been corrected according to Ref. 16. In terms of S

$$K^2 = 1 - \frac{\gamma + 1}{96S^2}\left(1 - \frac{8\gamma - 27}{24S} + \frac{754\gamma^2 - 757\gamma + 3615}{2880S^2} + \ldots\right) \quad (25)$$

Equation (25) has been shown[16] to give accurate results for $R = 0.625$ and lies within Stratford's[19] region of suggested true values for $R \geq 1.0$. Equation (25) is used herein to determine the relationship between r^* and r_1. Since the same mass flow passes through the throat and through the area of the spherical segment of radius r_1

$$A^* = 2\pi r_1^2(1 - \cos\omega) = \pi r^{*2}K^2 \quad (26)$$

or

$$R_1 = r_1/r^* = 0.5K \operatorname{coc}(\omega/2) \quad (27)$$

The fourth-degree polynomial that describes the axial velocity distribution for the throat contour may be written as

$$W = 1 + C_1\zeta + C_2\zeta^2 + C_3\zeta^3 + C_4\zeta^4 \quad (28)$$

where the coefficients and the distance $X_E = (x_E - x_I)/r_1$ are evaluated from the following conditions: at point I, $W = 1$, $W' = W_I'$, and $W'' = W_I''$; and at point E, $W = W_E$ from Eq. (1), $W' = W_E'$ from Eq. (5), and $W'' = W_E''$ from Eq. (7).

From these conditions

$$C_1 = X_E W_I' \quad (29)$$

$$C_2 = X_E^2 W_I''/2 \quad (30)$$

$$C_3 = 4(W_E - 1) - W_E'X_E - 3C_1 - 2C_2 \quad (31)$$

$$C_4 = -3(W_E - 1) + W_E'X_E + 2C_1 + C_2 \quad (32)$$

and

$$(W_I'' - W_E'')X_E^2 + 6(W_I' + W_E')X_E - 12(W_E - 1) = 0 \quad (33)$$

from which X_E may be evaluated. The value of x_E/r_1 is obtained from Eq. (2) for the selected value of M_E. Obviously

$$x_0/r_1 = x_E/r_1 - X_E - \epsilon/r_1 \quad (34)$$

The parameters used to determine the throat contour are R, ω, and M_E (or W_E). Although it is not apparent, these parameters are not completely independent. According to Hall's statement concerning the applicability of his transonic solution with the number of terms retained, a criterion was established for throat contours calculated from the axial velocity distribution of Eq. (28). Each contour should be examined to determine not only that its coordinates approximately follow a circle, parabola, or hyperbola for about one diam downstream of the throat but also that its second derivatives in the same region approximate those of a circle or hyperbola within the accuracy of the numerical methods used in the solution. For values of ω in the range from 8 to 12°, it has been found that this criterion was best satisfied if the coefficient C_3 from Eq. (31) was approximately equal to $W_I'''X_E^3/6$ where W_I''' was given by Eq. (23). This added requirement involves the iterative solution of the equation

$$W_I'''X_E^3 + 6W_I''X_E^2 + 6(3W_I' + W_E')X_E - 24(W_E - 1) = 0 \quad (35)$$

along with Eq. (33), since X_E and either W_E or R are initially unknown. Even with this added requirement, it appears that R should be limited to values between about 9 and 15 for $\omega = 12°$. Typical combinations of values of R and M_E are shown in Fig. 2 for three values of ω. As ω decreases, the allowable values of R increase.

For the downstream contour, Cresci[6] selected a third-degree polynomial to express the axial velocity distribution from point B to point C with the criteria that the first derivative at point B matched that for radial flow and that both first and second derivatives were zero at point C. Furthermore, the contours that he presented were for a Mach number increment $(M_C - M_B)$ of 0.2. If this increment is increased for a given design Mach number M_C, the magnitude of the second derivative of the velocity distribution, evaluated at the point B, decreases until a value is reached that matches the second derivative of the radial-flow distribution. At this point

$$W_C - W_B = -2(W_B')^2/3W_B'' \quad (36)$$

Cresci's value of Mach number increment was apparently satisfactory for the 50-in.-diam Mach 8 nozzle described in the Introduction. However, at high M_C's, if the characteristics from points B and C are traced upstream to points A and J (Fig. 1), the distance between points A and J becomes so small that it becomes practically impossible to machine the wall contour with the required accuracy. This problem was dramatically illustrated by Edenfield[15] for a Mach 20 nozzle.

For larger values of the velocity (or Mach number) increment, continuous curvature can be achieved by increasing the degree of the polynomial describing the velocity (or Mach number) distribution. With a higher order polynomial, care must be taken to insure that the second derivative is negative

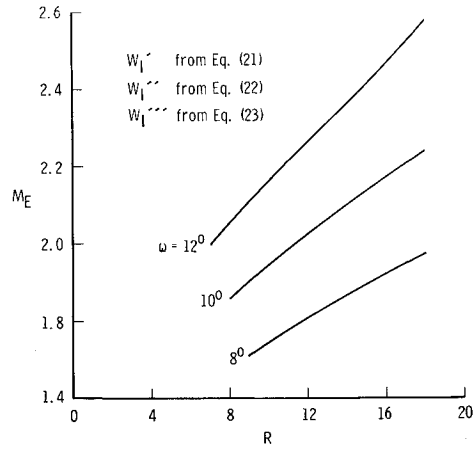

Fig. 2 Typical combinations of values of M_E and R.

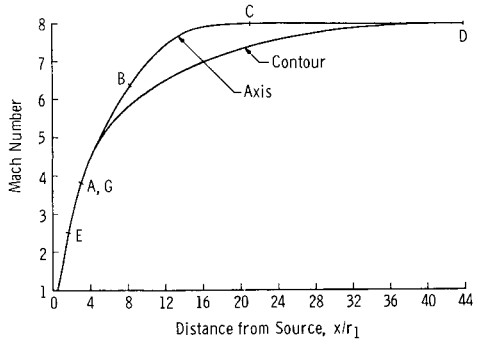

Fig. 3 Typical Mach number distributions for Mach 8 nozzle, M_C–M_B = 1.66.

at all points between point B and point C. As M_C increases, the velocity ratio approaches $k^{1/2}$, and the increment $(W_C - W_B)$ approaches zero. Thus, a fifth-degree polynomial in W may have a second derivative which does not behave as desired for high M_C's. Therefore, as in Ref. 5 a fifth-degree polynomial is used:

$$M = D_0 + D_1\xi + D_2\xi^2 + D_3\xi^3 + D_4\xi^4 + D_5\xi^5 \quad (37)$$

where the coefficients are evaluated for the six conditions: at point B, $M = M_B$, $M' = M_B'$ from Eq. (4), and $M'' = M_B''$ from Eq. (6); and at Point C, $M = M_C$, $M' = 0$, and $M'' = 0$.

From these conditions

$$D_0 = M_B \quad (38)$$

$$D_1 = (x_C - x_B)M_B'/r_1 \quad (39)$$

$$D_2 = (x_C - x_B)^2M_B''/2r_1^2 \quad (40)$$

$$D_3 = 10(M_C - M_B) - 6D_1 - 3D_2 \quad (41)$$

$$D_4 = -15(M_C - M_B) + 8D_1 + 3D_2 \quad (42)$$

$$D_5 = 6(M_C - M_B) - 3D_1 - D_2 \quad (43)$$

The total length of the complete nozzle, measured from the source, is

$$x_D/r_1 = x_B/r_1 + (x_C - x_B)/r_1 + 2\sin(\omega/2)(M_C - M_C^{-1})^{1/2}[(k - 1 + M_C^2)/k]^{k/4} \quad (44)$$

In Eq. (37), the distance $(x_C - x_B)/r_1$ is one of the parameters for use by the designer to adjust the length of the nozzle. Since the point B is at the end of the radial-flow region, x_B/r_1 is determined from Eq. (2) for the selected value of M_B, which is the other design parameter for the downstream contour to produce M_C. The contours presented by Yu[5] are based on

$$x_C - x_B = 2(r_C - x_B) \quad (45)$$

where r_C is calculated at M_C from Eq. (2), but somewhat more freedom can be allowed in the selection of parameters. A typical axial distribution of M is shown in Fig. 3 together with the resulting distribution along the inviscid contour.

The parameters $(x_C - x_B)/r_1$ and M_B are interdependent since the second derivative of Eq. (37) must be negative throughout the range from point B to point C. A thorough check of the second derivative should be made to insure its desired behavior. One means at the disposal of the designer to help insure its proper behavior is to reduce Eq. (37) to a fourth-degree polynomial by setting D_5, Eq. (43), equal to zero and solving the resulting quadratic equation for $(x_C - x_B)/r_1$:

$$(x_C - x_B)/r_1 = [-3M_B'/M_B''] \times \{1 - [1 + 4(M_C - M_B)M_B''/3M_B'^2]^{1/2}\} \quad (46)$$

Equation (46) has a solution only if

$$M_C - M_B \leq 0.75M_B'^2/(-M_B'') \quad (47)$$

Such a procedure places a lower limit on M_B and a corresponding upper limit on $(x_C - x_B)/r_1$, which in turn limits the distance from point A to point J on the contour. The severity of such limitations must be left to the discretion of the designer.

After the flow properties along characteristics EG, AB, and CD are determined analytically at the desired number of points from radial-flow considerations and along the axis from the prescribed velocity distributions, the characteristics method is used to determine the inviscid contours. For the throat region, the network starts at point E and progresses upstream. For the downstream section, the network starts at point B and progresses downstream. In general, the characteristic network extends beyond the wall contour, and the wall point on each characteristic can be determined by integrating the mass flow crossing it until the value is reached which is the same as that crossing EG (or AB). Downstream of point C, the integration is from C to a typical intermediate point K and thence to the wall to determine the location of point L. Generally, equiangular increments are selected on the radial flow characteristics and equidistant increments from point B to point C and from point C to point D. Upstream of point E, it has been found desirable to "stack" the increments closer together as point I is approached in order to keep the four sides of each individual net approximately equal. If point P represents the ith point of n segments between point I and point E, it is suggested that the ratio of distance IP to distance IE be $(i/n)^2$.

The characteristic network for the throat region terminates at the branch line IH. The small length of contour from the geometric throat (point T) to point H is essentially an arc of a circle of radius Rr^* if the throat parameters have been suitably selected. The equations in terms of S appear to be slightly better than those in terms of R. The transonic solution, as described, appears to be incompatible with the assumption that is sometimes made that $M_I'' = 0$. From differentiation of Eq. (1), it is found that

$$M_I' = [(\gamma + 1)/2]W_I' \quad (48)$$

and

$$M_I'' = [(\gamma + 1)/2][W_I'' + 3(\gamma - 1)W_I'^2/2] \quad (49)$$

When Eqs. (18) and (19), or Eqs. (21) and (22) are substituted into Eq. (49), it is found that $M_I'' > 0$ for all values of R for which the transonic solution is valid. In particular, if $W_I'' = 0$, then $M_I'' = 3M_I'^2/k$. Considerations such as these were not taken into account in the nozzle designs of Refs. 1, 2, and 12–14, but it would be extremely difficult to assess their influence on the quality of the flow in the test regions.

After the inviscid contour is obtained in nondimensional coordinates, each coordinate must be multiplied by a suitable scale factor (value of r_1) determined by the desired nozzle exit radius.

Boundary-Layer Correction

To each ordinate of the inviscid contour must be added the boundary-layer correction $\delta_a^* \sec \phi$ to obtain the physical contour of the nozzle. The following discussion will be limited to turbulent boundary layers. Although there are now considerably more experimental data on hypersonic boundary layers than were available approximately ten years ago when the first AEDC nozzle was designed, much more data are needed for accurate prediction of the boundary-layer growth, particularly at the higher hypersonic Mach numbers. Many correlations have been attempted to transform compressible data, obtained under conditions of heat transfer and longitudinal pressure gradients, to an equivalent

incompressible case. For wind-tunnel nozzles, the main correlations desired are the form factor $H = \delta^*/\theta$ and the skin-friction coefficient as a function of Reynolds number based on momentum thickness θ or distance x measured from a selected starting point.

The method to be described is based on obtaining a solution to the von Karman momentum equation written in the form

$$\frac{d\theta}{dx} + \theta\left[\frac{2 - M^2 + H}{M\{1 + [(\gamma - 1)/2]M^2\}}\frac{dM}{dx} + \frac{1}{y}\frac{dy}{dx}\right] = \frac{C_f}{2}\sec\phi \tag{50}$$

which is a differential equation of the form, $\theta' + \theta P = Q$. In the solution of this equation, it is assumed that the values of M, y, and $\phi = \tan^{-1}(dy/dx)$ are those obtained from the inviscid solution as functions of x. If values of H and C_f can also be found as functions of x (or functions of θ through iteration), Eq. (50) may be integrated numerically through repeated applications of the parabolic technique of integration

$$\theta_n - \theta_{n-2} = G_{n-2}\theta_{n-2}' + G_{n-1}\theta_{n-1}' + G_n\theta_n' \tag{51}$$

where

$$G_{n-2} = (2s - t)(s + t)/6s \tag{52}$$

$$G_{n-1} = (s + t)^3/6st \tag{53}$$

$$G_n = (2t - s)(s + t)/6t \tag{54}$$

and

$$\theta_n' = (d\theta/dx)_n = Q_n - P_n\theta_n \tag{55}$$

The integrating factors, Eqs. (52–54), reduce to the easily recognized values of Simpson's rule if $s = t$. Equation (51) assumes that only the nth values of θ and θ' are unknown, so that

$$\theta_n = (\theta_{n-2} + G_{n-2}\theta_{n-2}' + G_{n-1}\theta_{n-1}' + G_nQ_n)/(1 + G_nP_n) \tag{56}$$

The integration is started at the throat ($n = 1$) where it is assumed that $\theta_T' = 0$ and $\theta_T = Q_T/P_T$. At the throat, $P_T = (2 + H - M_T^2)(dW/dx)_T/W_T$, where[9]

$$W_T = 1 + 1/4R - (14\gamma + 15)/288R^2 + (2364\gamma^2 + 4149\gamma + 2241)/82944R^3 + \ldots \tag{57}$$

and

$$(dW/dx)_T = (\beta/r^*)[1 + 3/8R - (64\gamma^2 + 117\gamma + 54)/1152R^2 + \ldots] \tag{58}$$

or, in terms of S[16]

$$W_T = 1 + 1/4S - (14\gamma - 57)288S^2 + (2364\gamma^2 - 3915\gamma + 14337)/82944S^3 + \ldots \tag{59}$$

and

$$(dW/dx)_T = (\lambda/r^*)[1 + 7/8S - (64\gamma^2 + 117\gamma - 1026)/1152R^2 + \ldots] \tag{60}$$

At point H, ($n = 2$), the value of θ' is obtained by assuming that $\theta_H' = s\theta_3'/(s + t)$ and that $(\theta_H - \theta_T)/(\theta_3 - \theta_T) = s^2/(s + t)^2$; i.e., the parabola through the first three points is symmetrical about the vertical axis through point T. In general, the interval $x_H - x_T$ is considerably greater than the succeeding interval found from the characteristics solution. The form of the momentum equation, Eq. (50), and its solution are predicated on the assumption that the boundary-layer displacement thickness $\delta^* = H\theta$ is small compared to the nozzle radius. As indicated in Ref. 20, a transverse curvature correction can be applied to δ^* to give an axisymmetric displacement thickness

$$\delta_a^* = \delta^* + (\delta^{*2} + y^2\sec^2\phi)^{1/2} - y\sec\phi \tag{61}$$

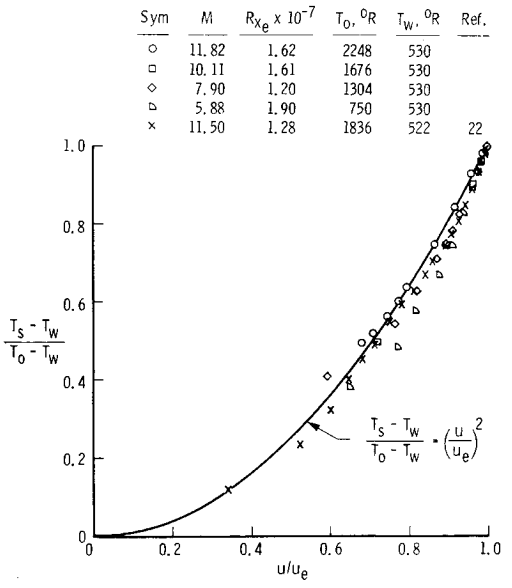

Fig. 4 Boundary-layer temperature profiles.

The evaluation of H involves some considerations of the boundary-layer temperature profile which may be approximated by the relation

$$\frac{T_s - T_w}{T_0 - T_w} = \frac{\alpha(T_{aw} - T_w)}{T_0 - T_w}\left(\frac{u}{u_e}\right) + \frac{T_0 - \alpha(T_{aw} - T_w) - T_w}{T_0 - T_w}\left(\frac{u}{u_e}\right)^2 \tag{62}$$

where α is, as yet, an undetermined factor. If $\alpha = 1$, Eq. (62) becomes the familiar quadratic of Crocco modified in an attempt to account for heat transfer and for Prandtl numbers other than one. If, on the other hand, $\alpha = 0$ or $T_w = T_{aw}$, Eq. (62) becomes parabolic

$$(T_s - T_w)/(T_0 - T_w) = (u/u_e)^2 \tag{63}$$

Intermediate values of α between 0 and 1 can be found such that Eq. (62) will fit several of the NOL temperature profiles presented in Ref. 21. On the other hand, Eq. (63) seems to fit better the temperature profiles measured in the AEDC hypersonic tunnels as shown in Fig. 4. Also shown in Fig. 4 is the temperature profile from Ref. 22 obtained in the gun tunnel at the University of Southampton. Although Eq. (63) fits these data quite well, it is much too simple an equation to be used close to the wall to correlate heat-transfer data. Neither can it be used to correlate the overshoot in local stagnation temperature found near the freestream edge of a boundary layer on an adiabatic wall. Equation (63) is useful for relating H with an equivalent incompressible factor H_i. By definition

$$\delta^* = \int_0^\Delta \left(1 - \frac{\rho u}{\rho_e u_e}\right)dy = \int_0^\Delta \left(\frac{T}{T_e} - \frac{u}{u_e}\right)\frac{\rho}{\rho_e}\,dy \tag{64}$$

and

$$\theta = \int_0^\Delta \frac{u}{u_e}\left(1 - \frac{u}{u_e}\right)\frac{\rho}{\rho_e}\,dy \tag{65}$$

In Stewartson's transformation[23]

$$\rho_0 a_0 dY = \rho a_e dy \text{ and } a_0 u = a_e U \tag{66}$$

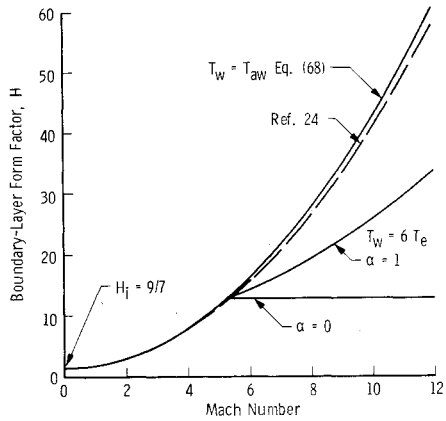

Fig. 5 Variation of form factor with Mach number.

In the boundary layer

$$(T_s - T)/(T_0 - T_e) = u^2/u_e^2 \tag{67}$$

If Eqs. (62, 66, and 67) are substituted in Eqs. (64) and (65), the relationship

$$H + 1 = T_w(H_i + 1)/T_e + \alpha(T_{aw} - T_w)/T_e \tag{68}$$

is obtained where by definition

$$H_i = \int_0^\Delta \left(1 - \frac{U}{U_e}\right)dY \Big/ \int_0^\Delta \frac{U}{U_e}\left(1 - \frac{U}{U_e}\right)dY \tag{69}$$

The influence of the value of α on values of H is illustrated in Fig. 5 for an incompressible value, $H_i = \frac{9}{7}$. For the adiabatic wall case where α has no effect, H increases rapidly with increasing M, and values calculated from Eq. (68) agree with those tabulated by Persh and Lee.[24] For a typical hypersonic wind tunnel where the test section wall temperature is approximately 540°R and the static air temperature is about 90°R, the value of H is independent of M if α is zero. Values of H determined experimentally in the AEDC tunnels tend to confirm this lack of a Mach number effect.

Fortunately, there appear to be compensating effects in the solution of Eq. (50) such that high values of H (for $\alpha = 1$) combine with low values of θ to give values of δ^* that are only a little higher, but consistently so, than those obtained when the parabolic temperature distribution is used.

In the determination of the compressible skin-friction coefficient from an equivalent incompressible value, use is made of the reference temperature concept. It is assumed that

$$(T'/T_e)C_f = C_{f_i} = 0.0773/(\log R_{\theta_i} + 4.563) \times (\log R_{\theta_i} - 0.546) \tag{70}$$

where

$$R_{\theta_i} = T_w\mu_e R_\theta C_f/T_e\mu_w C_{f_i} = T_w\mu_e R_\theta/T'\mu_w \tag{71}$$

and the relationship between C_{f_i} and R_{θ_i} is equivalent to that developed in Ref. 8 if the incompressible Reynolds number is based on momentum thickness. Equation (71) is Coles' law of corresponding stations.[25] The value of the incompressible form factor is related[8] to C_{f_i} by

$$H_i = [1 - 7(C_{f_i}/2)^{1/2}]^{-1} \tag{72}$$

In the solution of Eq. (50), an initial value of R_θ or R_{θ_i} is assumed to obtain C_{f_i}, C_f, and H. The calculated value of θ is used to obtain a new value of R_θ, and the process is iterated until the desired convergence is obtained.

The one remaining quantity which requires definition is the reference temperature T'. In general, the equation for T' may be written in the form

$$T' = B_1T_w + B_2T_{aw} + (1 - B_1 - B_2)T_e \tag{73}$$

Table 2 Experimental and calculated boundary-layer thicknesses

M	$R_{xe} \times 10^{-7}$	δ_a^*(exp), in.	$\delta_a^*(T')$, in.	$\delta_a^*(F_c)$, in.
6	8.2	1.51	1.37	1.48
8	5.9	2.37	1.96	2.06
10	5.5	3.25	3.01	3.13

Various authors[26–28] have suggested different values for the coefficients. For this form of the equation, the values suggested by Monaghan[28] become

$$B_1 = 0.54,\ B_2 = 0.16 \tag{74}$$

In addition, the factor F_c of Spalding and Chi[29] may be used as the ratio T'/T_e in Eqs. (70) and (71), although their factor for Reynolds number is different than that in Eq. (71). It may be noted that F_c was derived using the quadratic form ($\alpha = 1$) of Eq. (62). When the parabolic form, Eq. (63) was used to derive a modified value of F_c, it was found that such a modified value was independent of M in that it was a function only of T_w and T_e and appeared to give too much weight to T_e.

Comparisons of some experimental results, measured near the end of the AEDC nozzles, with calculated values are given in Table 2.

It can be seen that values calculated using F_c are consistently higher than those calculated using Monaghan's T' and agree better with the experimental values. The maximum discrepancy is about 17% for this range of conditions. Other combinations of factors were also tried in an attempt to improve the correlation. In particular, use of the Reynolds number factor of Spalding and Chi[29] gave consistently higher values of R_{θ_i} than Eq. (71) with resulting lower values of δ_a^*. Also, as mentioned previously, the use of $\alpha = 1$ in Eq. (68) gave consistently higher values of δ_a^*.

Certainly more work is needed to improve the accuracy of predicting the boundary-layer growth in hypersonic nozzles. Also, more experimental data are needed, not only near the end of the nozzle but also along the nozzle where the boundary-layer correction has the greatest influence on the Mach number gradient in the test region.

Concluding Remarks

Obviously, one particular operating condition (Reynolds number) must be selected for determining the correction to be applied to the inviscid contour. However, most wind tunnels are operated over a range of Reynolds numbers of the order of ten to one. The quality of flow in the test region should, therefore, be best near the design condition with some deterioration at other conditions. It is believed that this deterioration can be minimized by keeping the curvature of the contour continuous as described and by making the Mach number increment from point B to point C as large as feasible. Unfortunately, the expense of fabricating nozzles precludes a systematic experimental determination of an optimum nozzle design. Furthermore, lack of precision in the fabrication can often mask improvements which the designer hopes to achieve in the inviscid contour and/or the correction applied thereto to account for the boundary-layer growth. It is believed that adherence to the design techniques described will result in a satisfactory nozzle design.

References

[1] Owen, J. M. and Sherman, F. S., "Design and Testing of a Mach 4 Axially Symmetric Nozzle for Rarefied Gas Flows," Rept. HE-150-104, July 1952, Univ. of California, Institute of Engineering Research, Berkeley, Calif.

[2] Beckwith, I. E., Ridyard, H. W., and Cromer, N., "The Aerodynamic Design of High Mach Number Nozzles Utilizing

Axisymmetric Flow with Application to a Nozzle of Square Test Section," TN 2711, June 1952, NACA.

[3] Cronvich, L. L., "A Numerical-Graphic Method of Characteristics for Axially Symmetric Flow," *Journal of the Aeronautical Sciences*, Vol. 15, No. 3, March 1948, pp. 155–162.

[4] Foelsch, K., "The Analytical Design of an Axially Symmetric Laval Nozzle for a Parallel and Uniform Jet," *Journal of the Aeronautical Sciences*, Vol. 16, 1949, pp. 161–166, 188.

[5] Yu, Y.-N., "A Summary of Design Techniques for Axisymmetric Hypersonic Wind Tunnels," AGARDograph 35, Nov. 1958.

[6] Cresci, R. J., "Tabulation of Coordinates for Hypersonic Axisymmetric Nozzles Part I—Analysis and Coordinates for Test Section Mach Numbers of 8, 12, and 20," TN 58-300, Oct. 1958, Wright Air Development Center, Dayton, Ohio.

[7] Sivells, J. C., "Aerodynamic Design and Calibration of the VKF 50-Inch Hypersonic Wind Tunnels," TDR-62-230 (AD-299774), March 1963, Arnold Engineering Development Center, Arnold Air Force Base, Tenn.

[8] Sivells, J. C. and Payne, R. G., "A Method of Calculating Turbulent-Boundary-Layer Growth at Hypersonic Mach Numbers," TR-59-3 (AD208774), March 1959, Arnold Engineering Development Center, Arnold Air Force Base, Tenn.

[9] Hall, I. M., "Transonic Flow in Two-Dimensional and Axially-Symmetric Nozzles," *Quarterly Journal of Mechanics and Applied Mathematics*, Vol. XV, Pt. 4, 1962, pp. 487–508.

[10] Potter, J. L. and Carden, W. H., "Design of Axisymmetric Contoured Nozzles for Laminar Hypersonic Flow," AIAA Paper 68-372, San Francisco, Calif., 1968.

[11] Darwell, H. M. and Badham, H., "Shock Formation in Conical Nozzles," *AIAA Journal*, Vol. 1, No. 8, Aug. 1963, pp. 1932–1934.

[12] Johnson, C. B. et al., "Real-Gas Effects on Hypersonic Nozzle Contours with a Method of Calculation," TN D-1622, April 1963, NASA.

[13] Thickstun, W. R., Schroth, R., and Lee, R., "The Development of an Axisymmetric Nozzle for Mach 8," Paper 34, *Proceedings of the Fourth U.S. Navy Symposium on Aeroballistics*, 1958; also Rept. 5904, U.S. Naval Ordnance Lab, White Oak, Md.

[14] Enkenhus, K. R. and Maher, E. F., The Aerodynamic Design of Axisymmetric Nozzles for High-Temperature Air," NAVWEPS Rept. 7395, Feb. 1962, U.S. Naval Ordnance Lab, White Oak, Md.

[15] Edenfield, E. E., "Contoured Nozzle Design and Evaluation for Hotshot Wind Tunnels," AIAA Paper 68-369, San Francisco, Calif., 1968.

[16] Kliegel, J. R. and Levine, J. N., "Transonic Flow in Small Throat Radius of Curvature Nozzles," *AIAA Journal*, Vol. 7, No. 7, July 1969, pp. 1375–1378.

[17] Sauer, R., "General Characteristics of the Flow through Nozzles at Near Critical Speeds," TM 1147, June 1947, NACA.

[18] Sims, Joseph L., "Calculation of Transonic Nozzle Flow," TM X-53081, 1964, NASA.

[19] Stratford, B. S., "The Calculation of the Discharge Coefficient of Profiled Choked Nozzles and the Optimum Profile for Absolute Air Flow Measurement," *Journal of the Royal Aeronautical Society*, Vol. 68, April 1964, pp. 237–245.

[20] Potter, J. L. and Durand, J. A., "Analysis of Very Thick Laminar Boundary Layers in Axisymmetric High-Speed Fluid Flow," *Developments in Theoretical and Applied Mechanics*, Plenum, New York, 1963, pp. 341–360.

[21] Lobb, R. K. et al., "NOL Hypersonic Tunnel No. 4 Results; VII: Experimental Investigation of Turbulent Boundary Layers in Hypersonic Flow," NAVORD Rept. 3880, March 1955, U.S. Naval Ordnance Lab, White Oak, Md.

[22] Perry, J. H. and East, R. A., "Experimental Measurements of Cold Wall Turbulent Hypersonic Boundary Layers," Rept. 275, Feb. 1968, Univ. of Southampton, U.K.

[23] Stewartson, K., "Correlated Incompressible and Compressible Boundary Layers," *Proceedings of the Royal Society of London: Ser. A*, Vol. 200, 1949, pp. 81–100.

[24] Persh, J. and Lee, R., "Tabulation of Compressible Turbulent-Boundary-Layer Parameters," NAVORD Rept. 4282, May 1956, U.S. Naval Ordnance Lab, White Oak, Md.

[25] Coles, D., "The Turbulent Boundary Layer in a Compressible Fluid," *The Physics of Fluids*, Vol. 7, No. 9, Sept. 1964, pp. 1403–1423.

[26] Eckert, E. R. G., "Survey on Heat Transfer at High Speeds," TR 54-70, April 1954, Wright Air Development Center, Dayton, Ohio.

[27] Sommer, S. C. and Short, B. J., "Free-Flight Measurements of Turbulent-Boundary-Layer Skin Friction in the Presence of Severe Aerodynamic Heating at Mach Numbers from 2.8 to 7.0," TN 3391, March 1955, NACA.

[28] Monaghan, R. J., "On the Behaviour of Boundary Layers at Supersonic Speeds," *Fifth International Aeronautical Conference*, Institute of the Aeronautical Sciences, Inc., Los Angeles, Calif., 1955, pp. 277–315.

[29] Spalding, D. B. and Chi, S. W., "The Drag of a Compressible Turbulent Boundary Layer on a Smooth Flat Plate with and without Heat Transfer," *Journal of Fluid Mechanics*, Vol. 18, Pt. I, Jan. 1964, pp. 117–143.